Journal of Non-Crystalline Solids xxx (xxxx) xxx–xxx

Contents lists available at ScienceDirect

Journal of Non-Crystalline Solids

journal homepage: www.elsevier.com/locate/jnoncrysol

Effects of strain rates on shear band and serrated flow in a bulk metallic glass

Peiyou Li

School of Materials Science and Engineering, Shaanxi University of Technology, Hanzhong 723001, People's Republic of China

ARTICLE INFO

Keywords:
Bulk metallic glass
Shear band
Strain rate
Serrated flow

ABSTRACT

Effects of different strain rates on the shear band and serrated flow in $Ti_{30.81}Cu_{48.83}Ni_{7.44}Zr_{12.92}$ bulk metallic glass compressed at the room temperature were investigated. With increasing strain rates, the plastic strain, maximum compressive strength, and numbers and densities of shear bands increases, and the serrated flow in the second stage translates from similar uniformity to heterogeneity. No uniformity serrated flow in the second stage was found to be the combination of the no uniformity serrated flow in the first stage and the uniformity serrated flow in the second stage. The range of the stress drop in the second stage of the serrated flow coming from the discontinuous slip of the primary shear plane, is from 22 ± 1 MPa to 35 ± 1 MPa at different strain rates; the corresponding maximum value of stress drop is 35 ± 1 MPa. The range and maximum value of stress drop is crucial to further understand the mechanism of plastic strain in the metallic glass field.

1. Introduction

The long-range disorder and short-range order structure of bulk metallic glass (BMG) attribute different mechanical behaviors to BMG than that of the crystal with long-range order. In the compressive stress–strain curve of BMG at room temperature, the serrated flow is shown in the region of plastic deformation [1–5]. As early as in 1973, Chen et al. [6] reported that the serrated flow of BMG comprises two parts: the first part is the irregular serrated flow caused by the high local discontinuous shear band, and the second part is the uniformity serrated flow, originating from the propagation of a single shear band. The difference in the two parts is that the formation of shear band corresponding to the irregular serrated flow cannot be extended to the whole sample in the initial stage of deformation [7]. Wright et al. [8,9] assumed that each serrated flow corresponds to the independent shear band in the research of compressive deformation behavior of Zr-based BMG. The hypothesis of the formation and propagation of the single shear band is accepted and used to explain the deformation behavior of BMG in nanoindentation experiments [9,10]. Mukai et al. [11] found two different regions at the fracture, after the compression deformation of the Pd-Ni-P BMG. The first region is the slip of shear band, and the second region is the fast fracture of samples. Sergueeva et al. [12] pointed that the serrated flow is composed of the repeated slip of shear band along the primary shear plane in compressed Zr-based BMG at low strain rate. Song et al. [7] found that the main shear deformation is along the main shear plane under the conditions of low strain rate in the compressive deformation of Zr-based BMG. The macroscopic plastic of the compressed sample is caused by the slip of the sample in the stress–strain curve; actually, the macroscopic plastic is not uniform deformation, but results from the formation and extension of multiple shear bands [7]. They reported that the serrated flow is actually caused by the discontinuous slip of samples. In situ observation of the compressed sample indicates that the discontinuous slip of the sample corresponds to the serrated flow, and the shear band preferentially forms along the main shear plane. Recently, Sun et al. [13] reported the interaction of the shear band in five compressed Zr-based metallic glass samples simultaneously; the statistical analysis of the stress drop of serrated flow indicates that the incubation time of the serrated flow and the interactions of multiple shear bands are a complex process, and the multiple shear bands are more relevant than the single shear band.

In fact, the range of the stress drop of the discontinuous slip along the primary shear plane and the effect of different strain rates on the range of stress drop are still not very clear. In this study, the effect of different strain rates on the shear band and stress drop of the serrated flow was investigated for Ti-Cu-Ni-Zr BMG.

2. Experimental

The ingot of $Ti_{30.81}Cu_{48.83}Ni_{7.44}Zr_{12.92}$ (at.%) alloy with nominal composition was prepared by the arc-melting a mixture of pure metal elements (with the purity being 99.9%) in a titanium-gettered argon atmosphere. The ingot was re-melted at least four times to achieve the chemical homogeneity, and then suction cast into copper molds to form rod-like shape sample with a diameter of 3 mm. The phase of the sample was characterized by X-ray diffraction (XRD) equipped with Cu K_α radiation at an operating voltage of 30 kV, using the flakes of the 3-

E-mail address: lipeiyou112@163.com.

https://doi.org/10.1016/j.jnoncrysol.2018.01.012
Received 29 November 2017; Received in revised form 5 January 2018; Accepted 8 January 2018

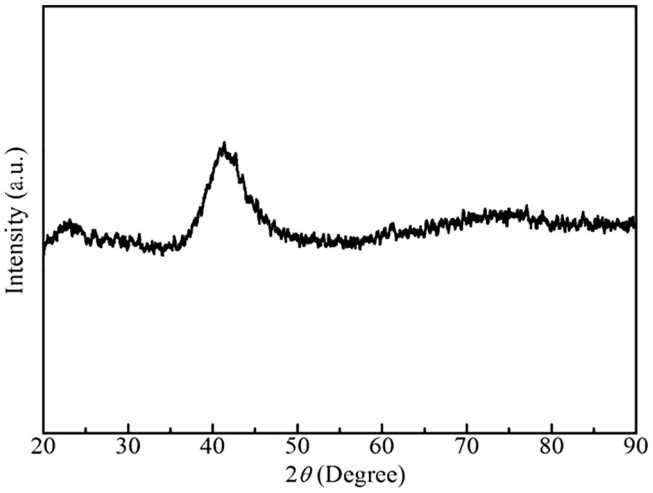

Fig. 1. XRD patterns of $Ti_{30.81}Cu_{48.83}Ni_{7.44}Zr_{12.92}$ alloy with a diameter of 3 mm.

mm-diameter cylindrical samples. Thermal analysis of samples with a diameter of 3 mm was carried out by differential scanning calorimetry (DSC) and differential thermal analysis (DTA), under continuous argon flow and at a heating rate of 0.33 K s^{-1} (Perkin-Elmer DSC 7). A cylindrical sample, with a diameter of 2 mm and a height of approximately 4 mm, was prepared from the as-cast rods for the uniaxial compression tests. The compression test was carried out at room temperature in a compression testing machine of CMT5105, at different strain rates of 2.54×10^{-4}, 4.25×10^{-4}, and 8.5×10^{-4} s^{-1}. After compression, the fracture surfaces were observed by scanning electron microscopy (SEM) using a JSM 6390LV SEM instrument.

3. Results and discussion

The compositions of the Ti-Cu-based Ti-Cu-Ni-Zr BMGs were designed by using the "proportional mixing of binary eutectic" method, as reported in literature [14]. In fact, the Ti-Cu-Ni-Zr BMGs comprise four deep eutectic units of $Cu_{73}Ti_{27}$, $Zr_{76}Ni_{24}$, $Ti_{76}Ni_{24}$, and $Cu_{62}Zr_{38}$. By adjusting the coefficient (x) of $Ti_{76}Ni_{24}$ and $Cu_{62}Zr_{38}$, the compositions (C_{am}) of Ti-Cu-Ni-Zr alloys can be expressed [14] as,

$$C_{am} = 0.55(Cu_{73}Ti_{27}) + 0.1(Zr_{76}Ni_{24}) + (0.25 - x)(Ti_{76}Ni_{24}) + (0.1 + x)(Cu_{62}Zr_{38}). \quad (1)$$

The glass forming ability is reported to be good when the Cu content is approximately 50% [4]. Therefore, in this study, when $x = 0.04$, the component of $Ti_{30.81}Cu_{48.83}Ni_{7.44}Zr_{12.92}$ alloy can be calculated.

The XRD pattern of $Ti_{30.81}Cu_{48.83}Ni_{7.44}Zr_{12.92}$ alloy with a diameter of 3 mm exhibits two broad diffraction peaks of amorphous phase, indicating that the $Ti_{30.81}Cu_{48.83}Ni_{7.44}Zr_{12.92}$ alloy is a typical fully amorphous phase, as shown in Fig. 1. To characterize the glass forming ability of the alloy, the DSC and DTA curves are shown in Fig. 2. Fig. 2a shows three peaks of crystallization, the glass transition temperature, T_g (678 ± 2 K); crystallization temperature, T_x (723 ± 2 K); the melting temperature, T_m (1099 ± 2 K); and liquid temperature, T_l (1169 ± 2 K) in Fig. 2b. In addition, the calculated supercooled liquid region of ΔT_x ($=T_x - T_g$) [15] and the γ ($=T_x/(T_g + T_l)$) value are equal to 45 ± 2 K and 0.391 ± 0.001, respectively, and are larger than the ΔT_x (26 ± 2 K) and the γ [16] (0.385 ± 0.001) of $Ti_{35.05}Cu_{49.64}Ni_{7.69}Zr_{7.6}$ BMG with a critical diameter of 2 mm [4], respectively, indicating that the present $Ti_{30.81}Cu_{48.83}Ni_{7.44}Zr_{12.92}$ BMG has a good glass forming ability. In addition, the reduced glass transition temperature T_{rg} ($=T_g/T_l$) [17] is 0.58 ± 0.01, which is smaller than that (0.591 ± 0.001) of $Ti_{35.05}Cu_{49.64}Ni_{7.69}Zr_{7.6}$ BMG [4], indicating that the glass forming ability is not related to the T_{rg} value. Accordingly, the results of XRD and thermodynamic parameters show that the present $Ti_{30.81}Cu_{48.83}Ni_{7.44}Zr_{12.92}$ BMG has the good glass forming ability in Ti-Cu-Ni-Zr alloy system.

Three $Ti_{30.81}Cu_{48.83}Ni_{7.44}Zr_{12.92}$ samples were compressed at different strain rates of 2.54×10^{-4}, 4.25×10^{-4}, and 8.5×10^{-4} s^{-1}, and the corresponding samples were labeled as S_I, S_{II}, and S_{III}, respectively. The stress–strain curves of these three compressive samples are shown in Fig. 3. The measured and calculated mechanical data are listed in Table 1. The plastic strain (ε_p) and the maximum compressive strength (σ_b) increase with increasing strain rates as shown in Fig. 3a; the ε_p and σ_b values range from 1.57 ± 0.02% and 2029 ± 10 MPa, respectively, at a strain rate of 2.54×10^{-4} s^{-1} to 19.0 ± 0.02% and 2390 ± 10 MPa, respectively, at a strain rate of 8.50×10^{-4} s^{-1}. In addition, compressed S_{II} sample has a larger elastic limit (σ_e), higher yield strength (σ_y), and higher Young's modules (E) of 1851 ± 10 MPa, 2147 ± 10 MPa, and 89 ± 2 GPa, respectively, compared to those of S_I and S_{II} samples.

At a low strain rate, the ductility of at room temperature BMGs is usually related to the number and density of shear bands [1,4,13]. The more the numbers and densities of shear bands are, the larger the plastic strains are for BMGs compressed at room temperature [1,4,13]. Therefore, different plastic strains at different strain rates in Fig. 3 can be explained from the numbers and densities of shear bands in Fig. 4. The second shear band of S_I sample is not found in the outer surface of the compressed sample in addition to the primary shear plane,

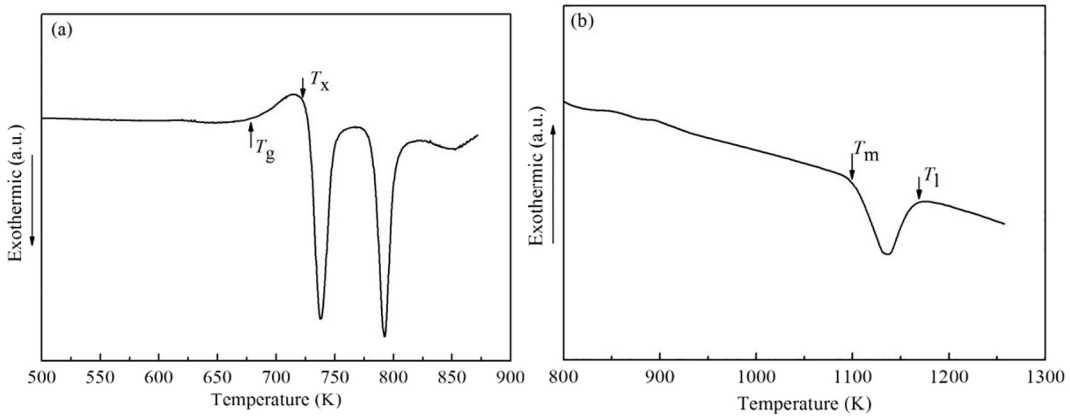

Fig. 2. DSC (a) and DTA (b) curves of $Ti_{30.81}Cu_{48.83}Ni_{7.44}Zr_{12.92}$ BMG with a diameter of 3 mm.